3.3.6 - Rainfall Data

All available rainfall data for the period from 1996 to 2002 were compiled and used as input for TIME. Stations with more than 3 years of nearly complete record (70 of 72 stations) were used to derive an annually averaged daily rainfall rate in meters (fig. 10). The distribution of annual average rainfall reveals that relatively less rainfall occurs near the southern boundary of Everglades National Park and relatively more rainfall occurs near its eastern boundary.

To account for these variations without attempting to achieve more spatial resolution than provided by the available data, six zones were defined and assumed to have spatially uniform rainfall (fig. 11). These zones were defined on the basis of annual average daily rates (fig. 10). The rainfall rate in each zone was computed as the simple arithmetic mean of all stations in the zone with existing data. The arithmetic mean may provide less than an optimal estimate, if the rainfall gage locations are clustered. Because of the small variation in average annual rates (fig. 10), clustering of gages was considered to be of little importance. The arithmetic mean is easy to apply, even when data with substantial gaps are used, and it does not require any area-weighting assumptions. A higher resolution spatial distribution of rainfall could not be derived due to the limited number of rainfall stations. A covariance-based kriging method was not suitable because of the lack of stations in western Everglades National Park. The average rates were calculated for 6-hourly periods using hourly data, when available, and uniformly parsed daily data otherwise.

An independent review by the Interagency Modeling Center of the model rainfall procedure led to another interpolation scheme using a dynamic Thiessen polygon method (DTPM). The SFWMD performed the interpolation and provided daily rainfall amounts in each cell. The following factors are relevant for comparing the techniques: (1) the previously mentioned sparseness of rainfall gages in the western part of the domain, (2) the limited accuracy of individual rainfall observations, (3) consistency with rainfall prescribed in the SFWMM, (4) the lack of any physical basis for preferring either interpolation technique, and (5) the small variations in the average rates (fig. 10). Based on these factors, there is no justification for preferring one interpolation technique over the other. A comparison of the cumulative rainfall for each of the six zones with the average rainfall computed from the cell-by-cell DTPM interpolated values is shown in figure 12. A close agreement was found in zones 1 to 4, with the DTPM giving somewhat more rainfall in zones 5 and 6.

The zonal approach applied in the SICS model domain area yielded results similar to those obtained using the DTPM cell-by-cell spatial interpolation. Results obtained with the TIME application do not indicate any problems that could be improved using the DTPM, and thus, the zonal rainfall scheme in TIME continues to be used. The average annual zonal rainfall ranges from 1.21 to 1.53 m; other techniques yield similar rainfall totals. The input file for zonal rainfall is named in appendix 2.

3.3.7 - Potential Evapotranspiration Parameters

Evapotranspiration (ET) rates were computed for the TIME simulation at 6 hour intervals based on the formulation described in section 2.3. The input file for evapotranspiration values is named in appendix 2. ET is a primary component of the water budget; therefore, a considerable effort was made to develop the Penman (eq. 1) and Penman-Monteith (PM) (eqs. 1 and 3, respectively) formulations to adequately describe ET in the TIME domain under historical conditions and under hypothetical conditions, such as those posed in CERP scenarios (U.S. Army Corps of Engineers and South Florida Water Management District, 2003). Because the average resistance of evaporative surfaces, r_s, and the aerodynamic roughness, z_o, cannot be determined from the set of measurements collected for vegetated sites, these variables are inferred indirectly. Tests indicated that when the aerodynamic roughness term z_o is small, the aerodynamic term in equation 2 becomes insignificant regardless of the value of r_s used. In all cases, this causes a substantial underestimation of actual evapotranspiration compared with the Bowen ratio method estimates (German, 2000). For larger values of z_o, the variables r_s and z_o were adjusted to produce a "best-fit," producing ET rates with the same mean as observations as well as the largest explained variance. When aerodynamic roughness z_o was increased, the r_s value corresponding to the best-fit formulation results increased and was no longer within the 100 to 300 s/m range of reasonable values (Eagleson, 1970; Oke 1978). This problem was resolved by noting that the ranges for z_o yielding reasonable values of corresponding r_s were centered around 0.05 m for all vegetated sites when water-heat storage was taken into account and was somewhat smaller when water-heat storage was ignored. Therefore, a z_o value of 0.05 m was selected for all vegetated sites, and r_s was adjusted to obtain the same mean ET as indicated by the data.

As part of the model calibration and evaluation procedure, a comparison was made between the calibrated PM model and a Priestly-Taylor (PT) formulation previously calibrated to the same measured data set (German, 2000). The data obtained from German (2000) were filtered to remove any bad data points caused by equipment errors or downtime. In the original regression analysis by German (2000) using the PT equation, all values other than those originally screened out were used. This included nighttime ET values, which were negligible. The obtained squared correlation coefficients were about 0.7, but improved to about 0.9 when transient soil and water-heat storage were accounted for in the net radiation term.

To compare the calculated and actual ET values, the mean of the values used in the model was adjusted to 1.12 m/yr. Therefore, the value of r_s was varied until the mean calculated and actual ET rates were identical. Tables 3 and 4 display (for each data filtering technique) corresponding r_s values and the percentage of explained variance (PEV) for z_o values of 1 and 5 cm at each site; PEV is defined as 1 - (residual variance)/(data variance) and is expressed as a percentage. Other values

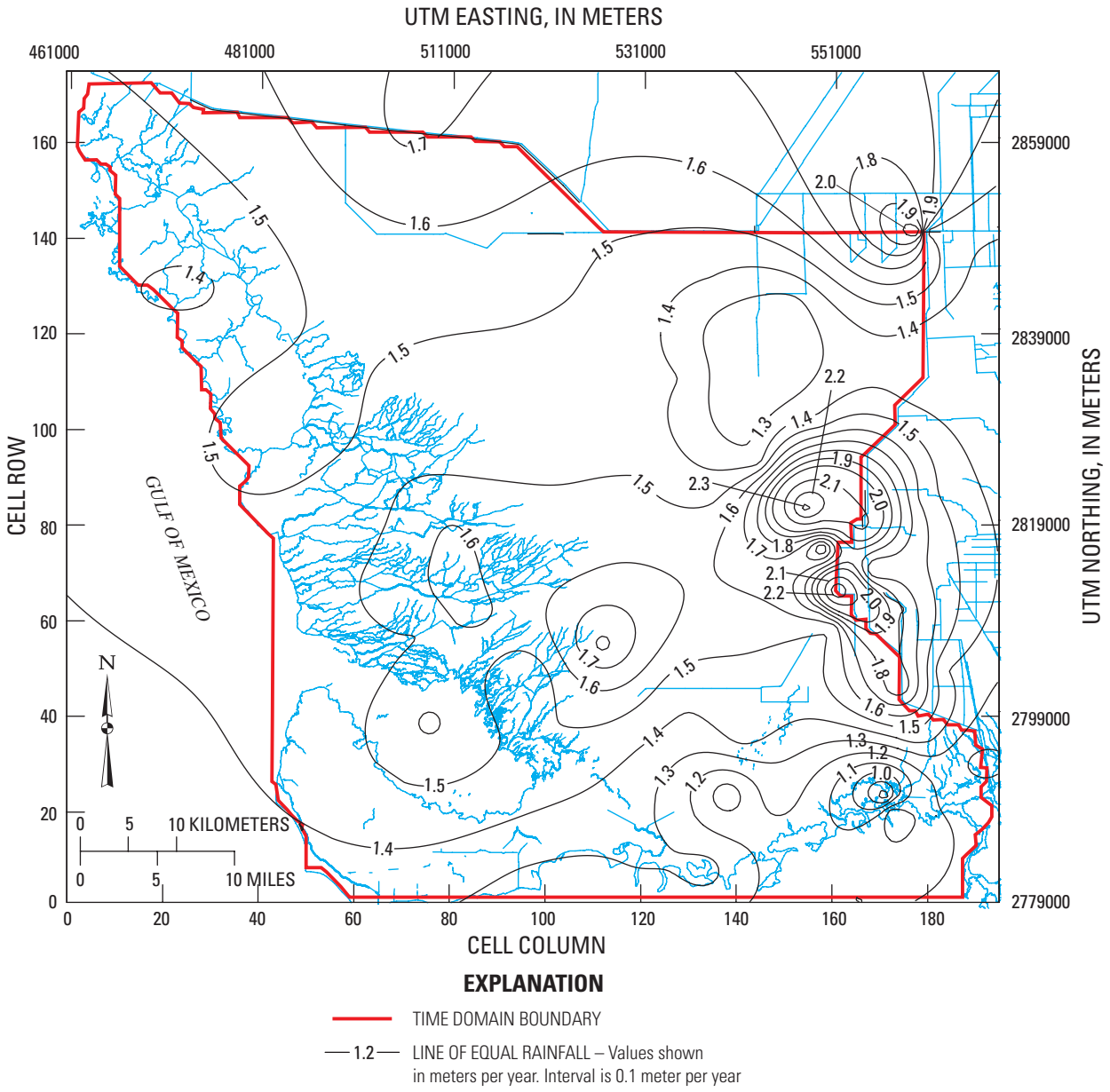

Figure 10. Distribution of annual average rainfall in the TIME area.

of z_o were tested, but produced r_s values that were outside the accepted range of values. Table 3 indicates that a z_o value of 1 cm generally results in a slightly higher PEV when water-heat storage is accounted for in the energy budget.

The just described calibration makes use of measured heat storage in the ponded water surrounding the vegetation. Specific measurements were made by German (2000) to estimate this component of the total energy budget. It is unlikely, however, that water-heat storage can be modeled in a predictive sense for this study. Ongoing advancements in utilizing air temperature for the prediction of water-heat storage (Shoemaker and others, 2005) may prove useful for future ET representation. Thus, the ability of the PM formulation to estimate ET was investigated when water-heat storage is not accounted for explicitly by adjusting net radiation. This is essentially a new PM formulation calibration that ignores water heat storage.

Table 4 shows ET values with full data filtration and without the adjustment to net radiation due to water-heat storage. This aerodynamic roughness comparison indicates

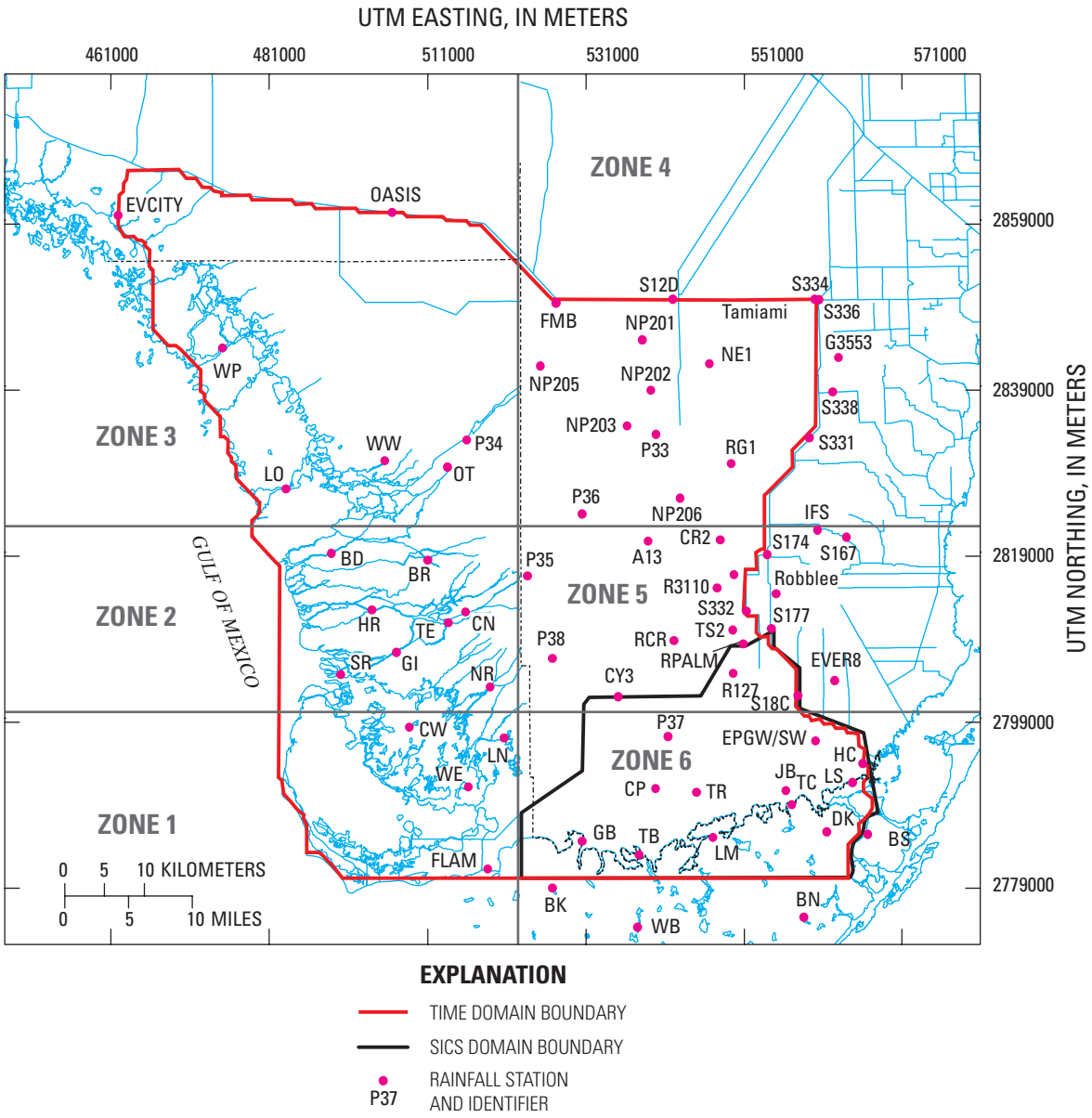

Figure 11. Location of rainfall stations within the rainfall zones of the TIME area.

that setting z_o to 5 cm yields the best results. Even though PEV typically decreased by about 20 percent, the PM method still explained a substantial part of the variance. As evidenced in table 4, the PT method yielded substantially poorer results in terms of total PEV. Water-heat storage data cannot be obtained for other time periods and hydrologic conditions. To preserve the mean ET rate, the calibration that ignores water-heat storage was used for ET modeling. The working assumption was that the calibrated model equation includes the average effect of heat storage in ponded water. The optimum r_s values obtained range between 128 and 165 s/m. The lower and upper values correspond to sites with sparse and dense vegetation, respectively. If the average r_s value for all vegetated sites was applied, however, PEV at individual sites decreased by only a few percent. It was not possible to distinguish individual site models from the average site model within the error bounds of the chosen ET formulation. Considering the other approximations and data uncertainty, a single r_s value, therefore, was applied across the entire vegetated modeling area.

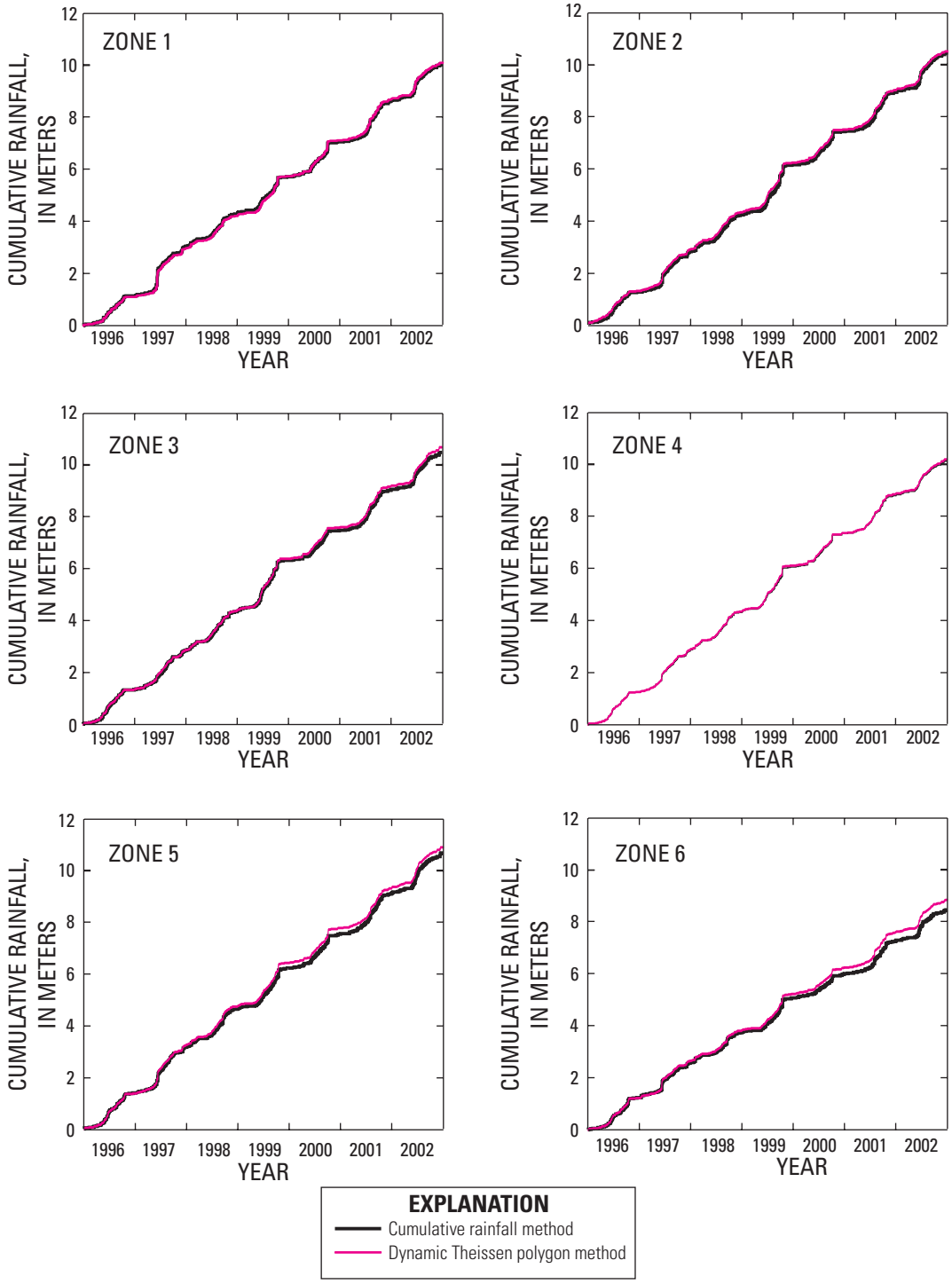

Figure 12. Comparison between cumulative rainfall for the six zones and average rainfall computed by the dynamic Thiessen polygon method. Zones are shown in figure 11.

Table 3. Calculated evapotranspiration values as a function of aerodynamic roughness (z_o) at vegetated sites in southern Florida.

[Site locations are shown in German (2000, fig. 1). r_s, average resistance of evaporative surfaces; PMPEV, Penman-Monteith method percentage of explained variance; PTPEV, Priestley-Taylor method percentage of explained variance]

Site	All data			Daytime data			Daytime data adjusted for water availability		
	r_s	PMPEV (percent)	PTPEV (percent)	r_s	PMPEV (percent)	PTPEV (percent)	r_s	PMPEV (percent)	PTPEV (percent)
z_o = 1 centimeter									
1	165	71.7	64.6	165	39.0	33.2	165	39.0	33.2
4	138	83.5	84.1	136	68.5	71.6	136	68.0	71.6
5	122	79.8	76.5	125	71.7	75.5	125	71.7	75.5
6	168	64.4	46.1	170	32.1	8.23	170	32.1	8.23
7	140	58.3	61.5	167	58.8	64.5	167	58.8	64.5
8	138	79.5	87.7	133	60.2	77.6	121	68.3	77.6
9	146	88.2	94.4	138	74.9	88.8	138	74.9	88.8
z_o = 5 centimeters									
1	146	71.3	64.6	143	38.4	33.2	143	38.4	33.2
4	132	81.6	84.1	127	64.8	71.6	127	64.4	71.6
5	120	77.6	76.5	120	65.6	75.5	120	65.6	75.5
6	150	65.3	46.1	147	33.3	8.23	147	33.3	8.23
7	138	52.1	61.5	157	51.2	64.5	157	51.2	64.5
8	132	75.0	87.7	126	52.1	77.6	116	61.0	77.6
9	133	84.7	94.4	123	68.6	88.8	123	68.6	88.8

Table 4. Calculated evapotranspiration values as a function of aerodynamic roughness (z_o) and water-heat storage.

[Site locations are shown in German (2000, fig. 1). r_s, average resistance of evaporative surfaces; PMPEV, Penman-Monteith method percentage of explained variance; PTPEV, Priestley-Taylor method percentage of explained variance]

Site	Daytime data adjusted for water availability without heat storage		
	r_s	PMPEV (percent)	PTPEV (percent)
z_o = 1 centimeter			
1	205	19.4	29
4	158	54.7	26.9
8	143	50.6	31.3
9	153	70	77.6
z_o = 5 centimeters			
1	165	23.4	29
4	140	56.4	26.9
8	128	51.1	31.3
9	131	66.1	77.6

This exercise revealed that the aerodynamic term is a significant factor. The significance of the aerodynamic term is indicated in the standard PT formula where its contribution is set to a constant that is about 26 percent of the net radiation term; however, this does not account for variability and dependence on wind speed and humidity.

To represent ET in a numerical model, the formulation must be constructed to function with only readily measurable quantities. To accomplish this, the stomatal resistance can be represented as a variable function of ponding depth and ground-water table elevation, both of which are readily measurable quantities. Aside from the difficulty in determining appropriate functional relations, this approach also requires that the PM equation be evaluated at every cell and for every time step during a model run.

Because this technique utilizes substantial computational effort, a simple depth function was derived that yields an estimate of actual evapotranspiration when factored with PM-calculated PET. Several functions were tested, including some that would decrease PET as the surface-water depth decreased to zero. The reanalysis, however, indicated that a near optimal approach (1) equated evapotranspiration to PET when the surface is wet, and (2) applied a factor equal to the greater of a calibrated value of 1.0 + depth/0.93 m or 0.0 when depth is negative. Physically, this relation corresponds to constant resistance when there is ponded water at the surface. When ponded water is absent under dry-surface conditions, water availability is limited by a calibrated root-zone depth of 0.93 m and a transpiration rate that decreases linearly with increased unsaturated zone depth. This is the approach used in the TIME application and in the final determination of r_s using the methodology described earlier. Finally, the results in tables 3 and 4 were produced using the actual ET calculation just described; therefore, the model calibration included the reduction of PET due to a lack of available water. This allows model estimates to be compared directly to measured ET rates.

An alternate test of the predictive formula ignores nighttime ET and applies the formula only during the active ET period. The PEVs in table 3 for each prediction formula are substantially smaller than those reported by German (2000). When nighttime values were included in the PM model (predicting zero ET and soil and water heat storage); however, results were obtained that are within 5 to 10 percent of those obtained using the PT approach.

The available data did not allow discrimination between the formulas for vegetated sites; therefore, the same formula was used for all of the vegetated sites. The cumulative ET is presented in figure 13, which shows a distinctive repeating annual pattern.

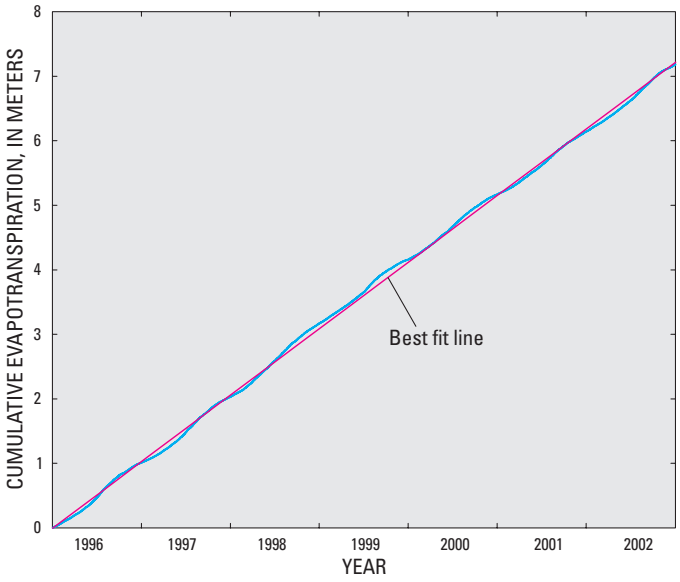

Figure 13. Cumulative evapotranspiration in the TIME area.

3.3.8 - Wind Data

Wind data obtained by German (2000) at an ET measurement site (OIH) along Old Ingraham Highway (fig. 1) are used as wind input in the TIME application. The record consists of 15-minute instantaneous data collected with a sensor 4 m above land surface. Gaps in the record were filled with data from Joe Bay Weather Station (JBWS) and Manatee Bay (MB) wind stations where necessary (fig. 1). JBWS is at the edge of Florida Bay, and thus, is more representative of winds over open water than OIH. Most wind speeds measured at OIH were about half of those measured at JBWS; therefore, it was possible to transform JBWS data by a constant multiplier and obtain reasonable estimates of OIH wind speeds using the same wind direction. The input file for wind stress is named in appendix 2.

Wind stress was calculated using a drag coefficient *WSTR* = 0.0018, and the following momentum flux formula:

$$\bar{\tau} = WSTR\ \rho_{air}\,|\overline{U}|\,\overline{U}\ , \qquad (4)$$

where ρ_{air} is the air density, and $\overline{U}$ is the wind velocity vector at 10 m above the surface. For computational efficiency, the wind stress was precomputed and input into the TIME application. The value chosen for the wind stress coefficient is more representative of stress over a vegetated land surface than over an open-water surface for relatively low (typically well below 10 m/s) wind speeds (Large and Pond, 1981).

3.3.9 - Coastal Water Levels and Salinities

Water-surface variations were prescribed along the open marine boundaries of the TIME application. The sparse measured data and the absence of a coastal hydraulic model necessitated the following approach. Harmonic constants for the three principal tidal components (*M2*, *O1*, and *K1*) were obtained from preliminary results of the Florida Bay model (J. Hamrick, TetraTech, written commun., 2005).

Seven separate boundary locations (fig. 1) were defined for the TIME simulation, corresponding to: (1) the boundary along Florida Bay; (2) the boundary encompassing Ponce De Leon Bay and the Harney and Broad Rivers; (3) Lostmans River; (4) Chatham River; (5) Lopez River; (6) Turner River; and (7) Barron River. For each of these boundaries, the Florida Bay model results were used to specify a mean level and the amplitude and phase of the *M2*, *O1*, and *K1* components. These boundaries are defined in the main input file for the surface-water simulation listed in appendix 2.

In addition to tides, low frequency sea-level variations were incorporated into the marine boundary conditions. Data from the USGS Trout Creek station were used because the record is reasonably complete for the 7-year period. A 30-day moving average was then computed, and yielded a final record with a mean of 0.518 m. The beginning and end values were made to agree by including the beginning of the dataset to compute the moving average at the end, allowing run continuation. Once the mean was subtracted, the moving average is added to the boundary levels computed by the tidal components to account for the low frequency sea-level variations. The input file for low-frequency tidal fluctuations is listed in appendix 2.

Boundary salinities are set to a constant value of 36 psu (practical salinity units) during flood flow. During the ebb flow, no value is prescribed and salinity at the boundary is computed based on values in the interior of the model grid. The return period for constituents that leave through the boundary was set to 60 minutes. These salinity boundaries are defined in the main input file for the surface-water simulation listed in appendix 2.

3.3.10 - Ground-Water Boundary Conditions

Ground-water flow is continuous across the northern and eastern domain boundaries. To simulate this flow, general-head boundaries (GHBs) are prescribed for the FTLOADDS ground-water component SEAWAT. The stages for these GHBs are interpolated from recorded stages at the Barron, S-333, S-334, S-336, G-211, Humble, G-789, Robblee, and Ever3 sites (fig. 9). An estimated conductance of 35,000 m/d was obtained by assuming local conductivity = (distance × cell width × layer thickness)/cell width, where local conductivity = 3,000 m/d (Langevin and others, 2004), distance = 300 m, cell width = 500 m, and layer thickness = 7 m. The input file for these GHB boundaries is named in appendix 2.

The marine boundaries are set as closed (no-flow) boundaries, which is justified as follows: (1) there is probably no freshwater flow through these boundaries because the salt front is located far inland (Fitterman and others, 1999); (2) some of the exchange that would occur at the lateral marine boundary instead occurs through the surface when the boundary is closed; and (3) it would be difficult to have an open boundary because of the need to specify ground-water flows or ground-water heads and salinity.

3.4 - Freshwater Flux Output at the TIME Application Boundary

One primary objective of the TIME application is to provide freshwater outflow to the coast so that the Florida Bay model (EFDC) can calculate resulting salinities. Because the EFDC model is separate from the TIME application, a method to transfer information at their interface is needed. The interface must be simplified because the models differ in structure (one being two-dimensional horizontal and the other three dimensional) and use different spatial discretizations. Fundamentally, the fluxes of water volume, momentum, and salt anywhere along the interface should be matched in the two models to satisfy continuity and conservation of salt laws in which total salt flux is the sum of advective and diffusive fluxes. Although this may be the best approach to use, a simpler method has proven to be successful in situations where the water-volume flux is small compared to offshore volume. The boundary in the bay model is represented with zero momentum and salt fluxes and with water volume flux equal to an equivalent volume of freshwater, which is applied as a zero-salinity source like rainfall.

The flow exchange between TIME and the EFDC is approximated by an equivalent freshwater flux. If the flow at a given instance from the TIME domain along the coast is q with salinity S, and q is small compared to ambient flows, then it effectively is equivalent to adding an amount of pure freshwater, q_f, equal to $q(S_0\text{-}S)/S_0$, where S_0 is a reference ocean salinity.

The salinity S is the salinity of the source water; that is, S is the salinity of the TIME domain cell just inside the boundary when flow is to the coast and S is the salinity of the boundary cell when flow is from the coast. The reference ocean salinity S_o represents an ambient open-water salinity, nominally set to 36 psu for the TIME application. Conceptually, S_o is the global reference for the fractional reduction or increase in salinity when water is added or removed from the offshore area.

The TIME application boundary freshwater flux computed by $q_f = q(S_0\text{-}S)/S_0$ is passed to the EFDC model as a volume of zero-salinity water. Figure 14 presents the four cases involved in the computation of q_f. A positive q_f represents flow to the offshore area when the inland water is less saline than the reference ocean salinity (case 1) or flow to the inland area when the offshore waters are more saline than the reference ocean salinity (case 2). A negative q_f represents flow to the inland area when the offshore is less saline than the reference ocean salinity (case 3) or flow to the offshore area when the inland waters are more saline than the reference salinity (case 4).

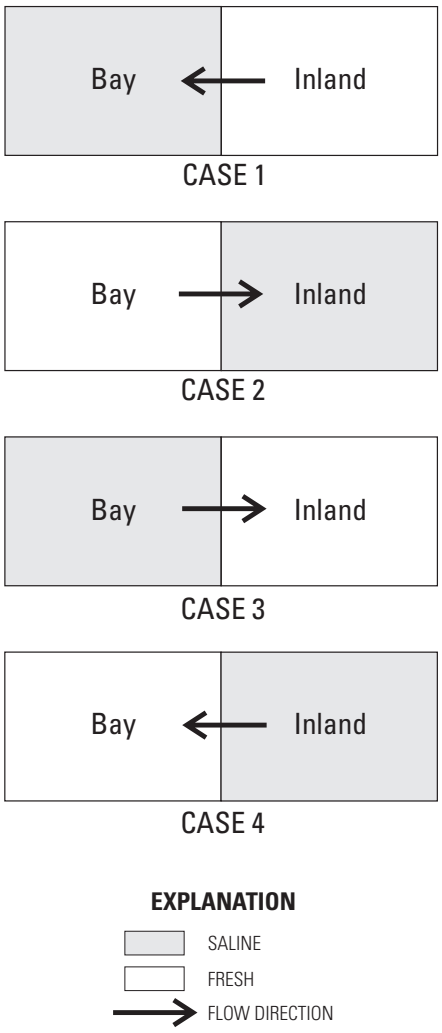

Figure 14. Freshwater flux cases.

3.5 - Model Initialization

The TIME application was initialized with water levels and salinities from a 1-year run for 1999. This year was chosen as a warm-up period because stages at the end of 1999 and the beginning of 1996 have similar water levels and flows. Surface-water flows and stages adjust relatively rapidly (within 3 to 4 months) to prescribed boundary conditions. Therefore, running the model for a full year was expected to create realistic surface-water conditions that are independent of starting conditions.

The ground-water model was initialized using ground-water heads set to 1 m below NAVD 88 and salinity values that approximate data from Fitterman and Deszcz-Pan (1998). The ground-water heads and flows reach reasonable values in about a month; however, salinities are much slower to adjust and can require decades to approach equilibrium under steady-state boundary conditions.

3.6 - Initial Model Calibration

More than 140 seven-year runs were made in the initial calibration of the TIME application. Adjustments were made to correct for errors in the initial input of boundary locations and Taylor Slough topography. Other adjustments were made to include features that were represented inadequately in the initial model input. These include river characteristics, roads, the Buttonwood Embankment, aquifer hydraulic conductivities, primary and secondary storage coefficients, conductivity of the surficial thin layer, and Manning's *n*. The parameters of the final model are contained in the FTLOADDS input files listed in appendix 2.

Additionally, the initial calibrated run (142) uses wind data from the Old Ingraham Highway (OIH) station (fig. 1) with no reduction in wind forcing due to the sheltering effect of vegetation. The thin layer over which leakage is calculated was given a conductivity of 0.004 m/d, with the underlying aquifer vertical conductivity of 1.0 m/d.

3.6.1 - Wetlands Water Levels

The model calibration uses stage values recorded at 105 different locations within the TIME domain. The following stations were chosen for graphical representation because of their extensive coverage of Shark River Slough and relatively complete data records: G-620, NE2, NP201, P33 to P38, and RG1 (figs. 9 and 15). At the beginning of 1996, simulated stages compare well with measured stages and relatively few stations show abrupt changes in stage; both characteristics support the chosen strategy of warming up the model using 1999 hydrologic conditions. The fit between measured and simulated data for each of the preceding sites is varied substantially and discussed herein.

The measured data fit simulated ground-water data better than simulated surface-water data at G-620 (fig. 15A). The ground-water head is below surface-water stage during most of the period, indicating downward leakage. Two major declines in ground-water head that occurred during the 2001 and 2002 dry seasons were simulated poorly by the model. The mean bias, correlation, and PEV are -0.004 m, 0.928, and 85.7 percent, respectively. The PEV for stage data is calculated as 1.0 – [Var(measured stage – simulated stage)/Var(measured stage)] and measures how well the model represents water-level fluctuations around a mean.

The visual fit between measured and simulated stage at NE2 (fig. 15B) is not as close as at G-620, primarily because of a bias in the mean, although all major ponding, accumulation, and depletion events are captured well. Simulated ground-water head is mostly lower than simulated surface-water stage and is in better agreement with measured head. The model land-surface altitude is apparently too high, which is confirmed by the data. The mean bias, correlation, and PEV are -0.11 m, 0.863, and 65.2 percent, respectively.

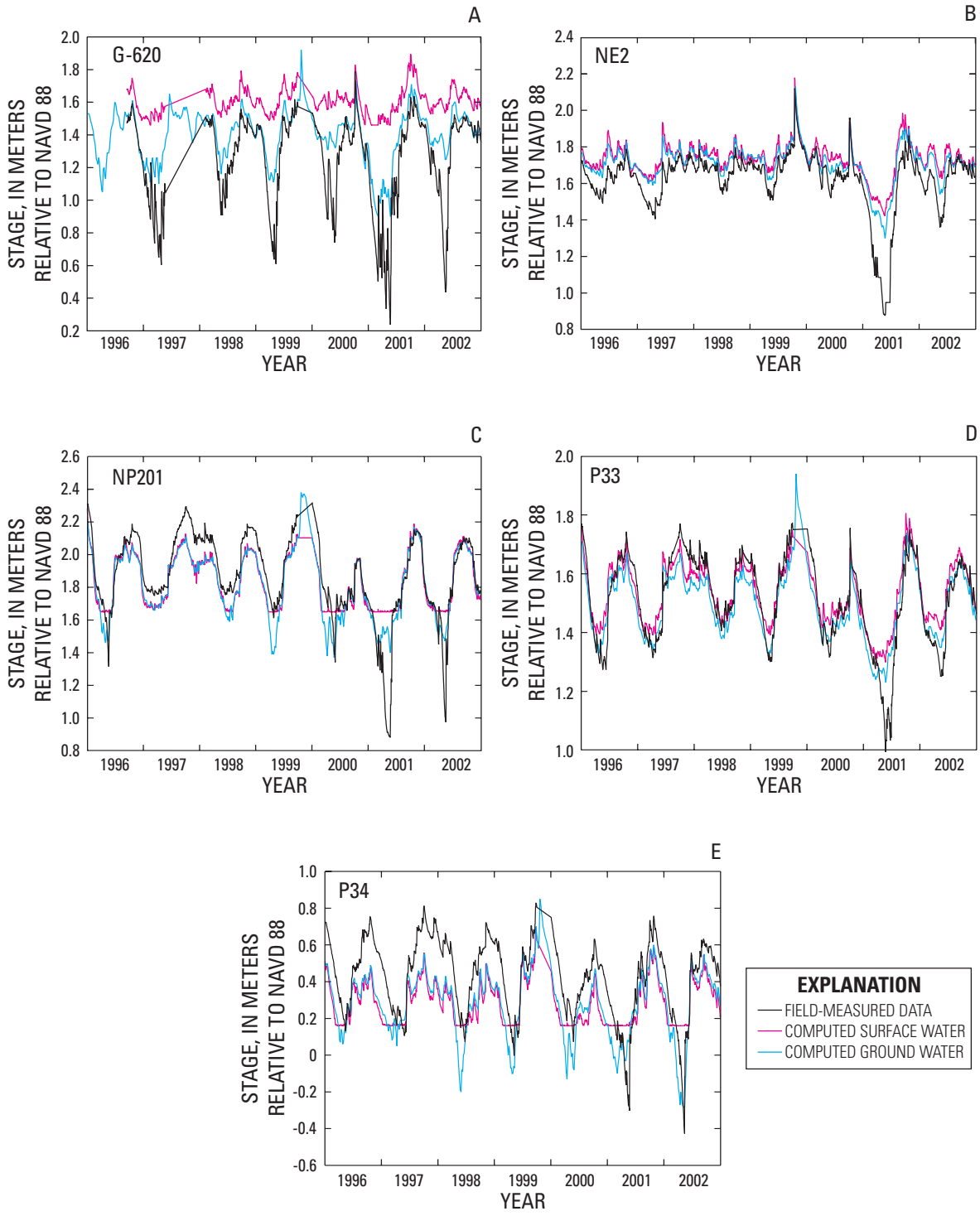

Figure 15. Comparison of water levels at selected gaging stations in the TIME area. Site locations are shown in figure 9.

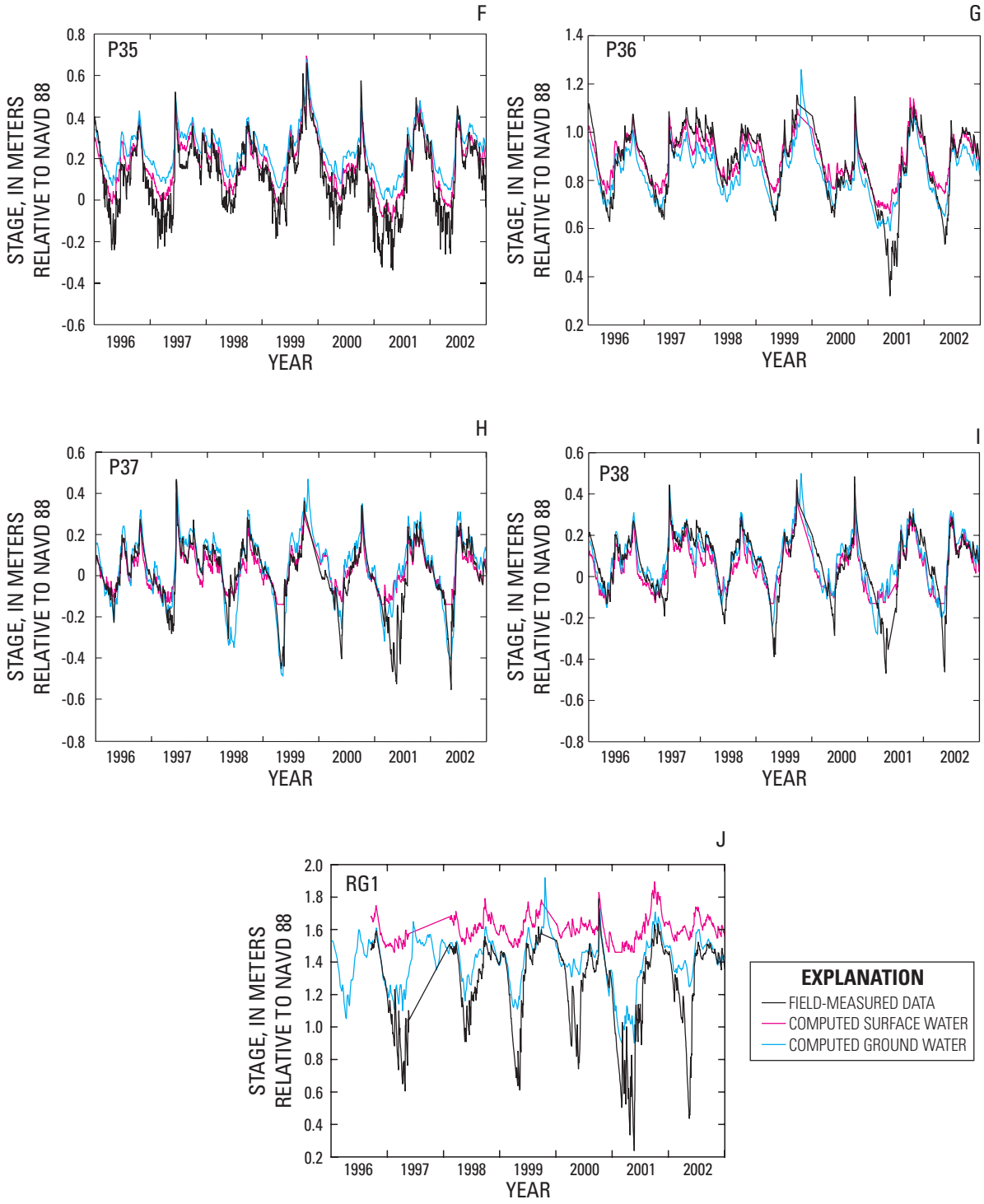

Figure 15. Comparison of water levels at selected gaging stations in the TIME area. Site locations are shown in figure 9.—Continued

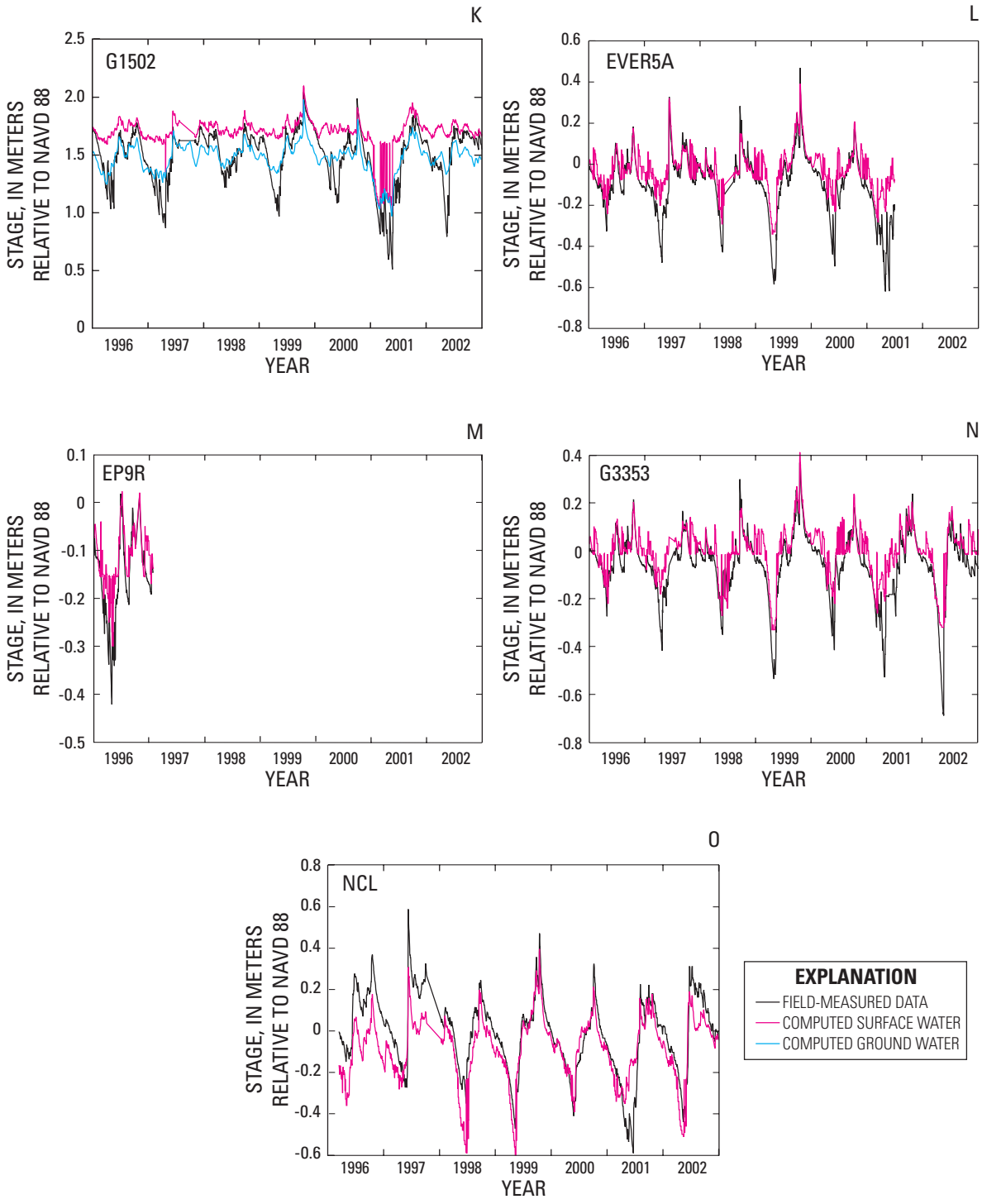

Figure 15. Comparison of water levels at selected gaging stations in the TIME area. Site locations are shown in figure 9.—Continued

Visual comparison of NP201 stages (fig. 15C) shows a mean shift during the first 4 years, followed by close agreement of measured and simulated surface-water stage. The two major declines in ground-water head are not well simulated, perhaps warranting an adjustment to the ground-water storage coefficient. The reason for mean shift is unclear, and by itself, might indicate a data problem; however, similar conditions at other stations indicate a more regional effect. At NP201 the model land-surface altitude is 0.23 m above measured land-surface altitude at the gage. The mean bias, correlation, and PEV are 0.04 m, 0.855, and 71.0 percent, respectively.

Stage at P33 (fig. 15D) shows a mean shift similar to NP201, but much smaller. The measured data fit simulated surface-water stage better at high water levels and simulated ground-water heads better at low water levels. The ground-water declines in 2001 and 2002 are much deeper at NP201, than P33, possibly indicating that they are caused by drainage to the east. The mean bias, correlation, and PEV are -0.02 m, 0.919, and 79.6 percent, respectively. The closeness of the agreement at P33 and its occurrence in the middle of Shark River Slough lend support to model performance in this part of the domain.

Measured trends at P34 (fig. 15E) are represented by the model data, but there is substantial bias in the mean. The shift during the first 4 years is evident at this site, although the ground-water level declines in 2001 and 2002 are simulated more accurately at this site than in preceding cases. Because model land-surface altitudes have no obvious errors, the bias may indicate a local frictional problem (discussed in section 3.7.2). The mean bias, correlation, and PEV are 0.16 m, 0.855, and 71.6 percent, respectively. Simulated ground-water head and surface-water stage agree closely throughout most of the wet season.

The surface-water hydrograph fit at P35 (fig. 15F) is closer than at most other sites; in this case, ground-water head is mostly above surface-water stage, indicating upward leakage. The mean bias, correlation, and PEV are -0.058 m, 0.947, and 88.2 percent, respectively. The surface-water fit at P36 (fig. 15G) is also closer that at most other sites. In this case, simulated ground-water head is mostly below simulated surface-water stage, and the fit to measured water-level data is best during low-stage conditions. The mean bias, correlation, and PEV are -0.02 m, 0.908, and 79.7 percent, respectively.

Measured and simulated stage closely correspond at P37 and P38 (fig. 15H, I), with ground-water head mostly above surface-water stage at both sites. The mean bias, correlation, and PEV are -0.01 m, 0.866, and 73.6 percent, respectively at P37; these same parameters are 0.02 m, 0.849, and 71.5 percent, respectively, at P38.

At RG1 (fig. 15J, Rocky Glades), simulated ground-water head agrees closely with measured stage. The 0.4-m discrepancy between the land-surface altitude measured at the gage and that measured by the topographic survey indicates the gage is located in a shallow depression, and that its measurement is more representative of ground-water head. The mean bias, correlation, and PEV statistics are -0.347 m, 0.673, and 40.4 percent, respectively. These statistics would improve substantially if simulated ground-water head is compared to measured stage instead of surface-water stage.

Although other stage records were not examined in the same detail, all were included in the calculation of model performance statistics. The model performance statistics consist of: (1) overall measured data mean; (2) measured data standard deviation; (3) overall model mean; (4) model standard deviation; (5) correlation between measured data and model output; (6) difference in means (DIFMEAN) (1) – (3); (7) difference in standard deviations; (8) PEV; (9) number of points used for calculations; (10) land-surface altitude defined for model cells; and (11) land-surface altitude as measured adjacent to the water-level gage.

The correlation between measured and simulated data is calculated with the mean removed from the series. The difference in means is a measure of the bias between the data and the model. Only quality-approved measured data values and their corresponding simulated values are used; missing data points are ignored in data and model statistics. Simulated ground-water head is used when model surface-water stage drops below the criteria for a semidry state described in section 2.2.1. The land-surface altitudes (items 10 and 11 noted earlier) are included to indicate, when elevations differ, whether extra care is needed to interpret the results (for example, RG1, fig 15J).

Surveying water-level gages to datum is difficult in the terrain of the TIME domain. The quality of the leveling at some stations has been found to be poor. Many of the field gages do not have a known land-surface altitude, and the following sites have not been referenced to a vertical datum: BD, BR, CN, GI, HR, LN, LO, NR, SR, TE, WE, WP, and WW (fig. 9). The summary statistics of stage comparisons for all 105 gages are listed in table 5.

Table 5. Summary statistics of stage comparisons for station data used in the TIME application.

[TIME, Tides and Inflows in the Mangroves of the Everglades]

Simulation run	Sum of absolute mean difference (meters)	Sum of squares of mean difference (meters^2)	Sum of correlations (percent)	Sum of explained variance (percent)
139	23.880	19.211	79.283	38.716
142	23.896	19.293	77.432	31.86
143	23.947	19.256	78.297	37.043
145	28.352	22.129	69.499	-5.352
146	23.259	19.022	76.794	38.547
157	22.088	18.195	81.141	39.687
157GW	19.725	17.454	83.179	54.038

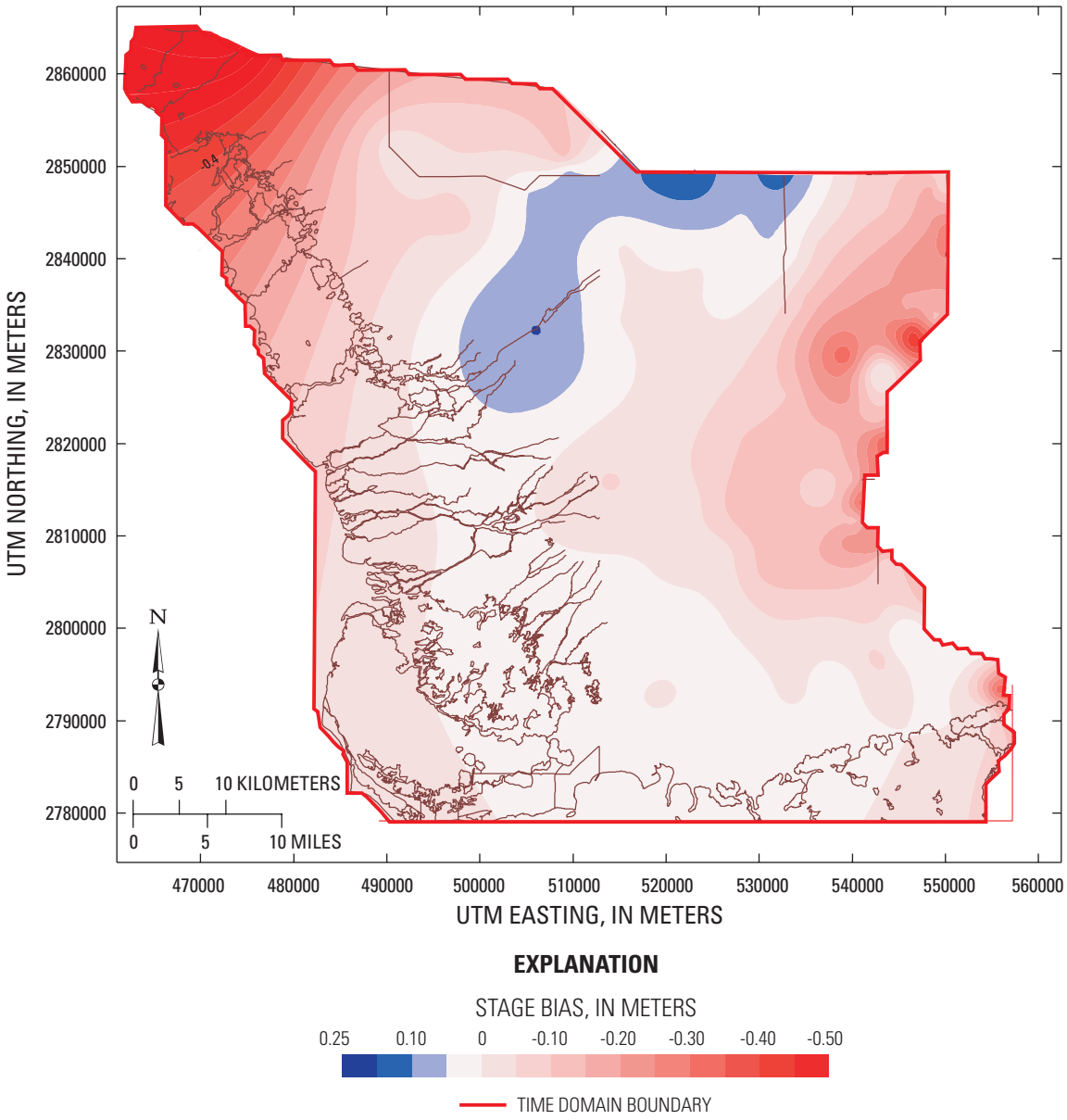

Figure 16. Spatial distribution of model mean stage bias in the TIME area for run 142.

Figure 16 shows the spatial distribution of the mean measured water level minus simulated water level (DIFMEAN); illustrating the spatial distribution of mean bias. Only stations referenced to a vertical datum were used to construct this map. The large negative bias in the north-western corner of the model is due to one gage (BICYA8) that is close to the model boundary (fig. 9). Unfortunately, there is no measured land-surface altitude for this gage to allow comparison with model topography. It is possible that a small river drains the area but is not accounted for in the model topography. Further investigation is needed to resolve this problem, which is confined to a small region of the domain.

The mean stage south of the S-12A, B, C, and D structures, and near P34, are somewhat lower than predicted, whereas stages near Levee-31 are somewhat higher than predicted (locations in fig. 9 and values in figs. 15E, J). This could indicate that the actual frictional resistance within the intervening area is less than that represented in the model. The bias for the ground-water stations, most of which are on the eastern side of the model domain, is generally larger than for surface-water stations and may influence contour locations in figure 16. This may be due partly to the effect of the storage coefficient, which has not been calibrated extensively in the model.

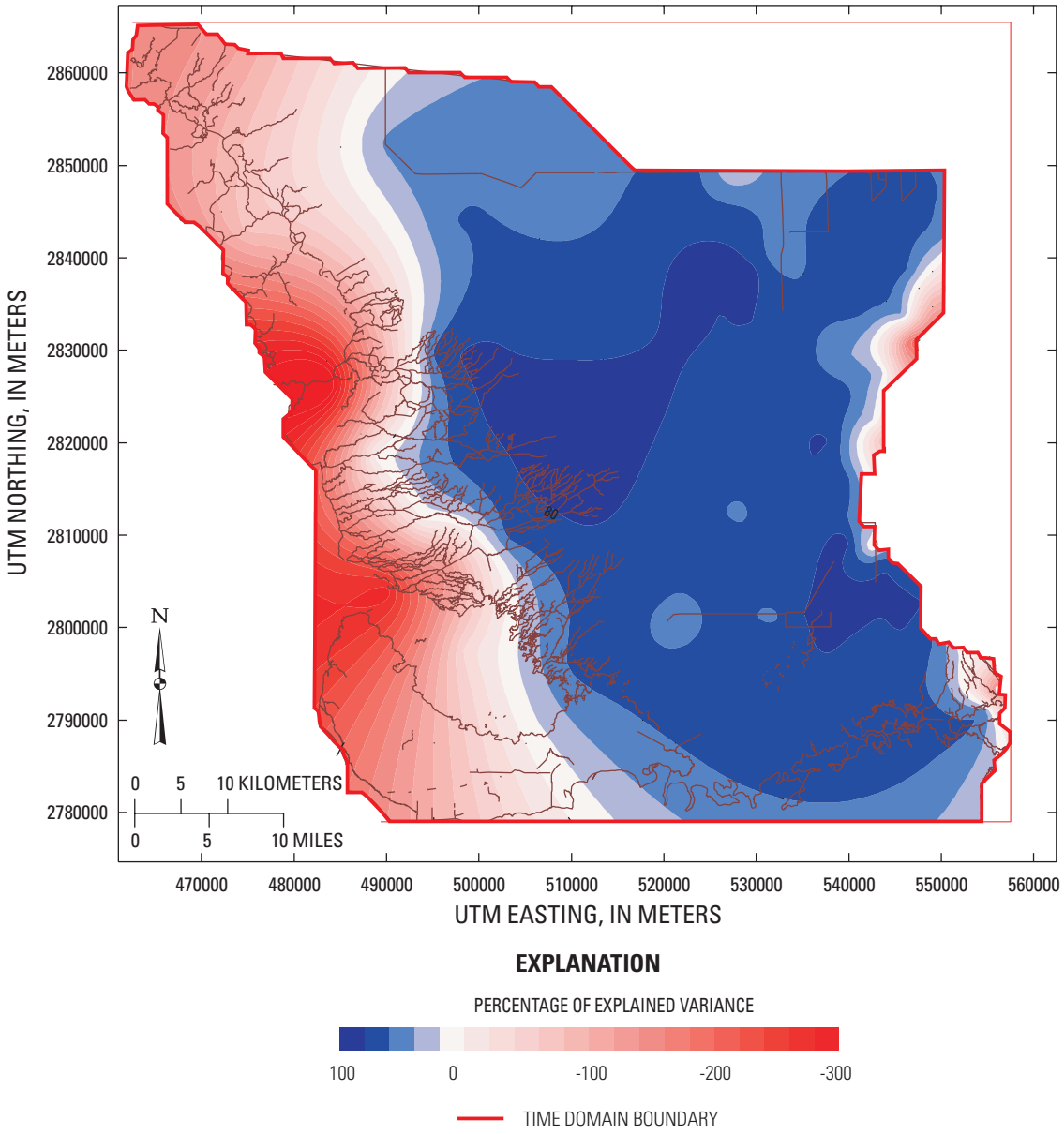

Figure 17. Spatial distribution of percentage of explained variance in the TIME area for run 142.

A contour map of the PEV for stage shows values ranging from 60 to 90 percent in most of the nontidal marshes (fig. 17). The PEV is lower in the tidal areas because relatively small errors in model tides result in large decreases in PEV. Small or negative PEV values occur near the northeastern edge of the domain where prevalent dry-surface conditions make simulations more difficult and dependent upon accurate topography. The negative PEV values in the C-111 Canal area, where the mean bias also is negative, indicate that modeled drainage may need some improvement; but tidal response is probably poor as well. The negative bias indicates mean model stage is greater than mean measured stage. The prescribed tide in northeastern Florida Bay obtained from the preliminary bay model has an *M*2 amplitude of 0.03 m, which is known to be too large.

3.6.2 - West Coast River Stages and Flows

Direct comparisons of measured and simulated stage at the USGS west coast river stations is considered problematic because of difficulties associated with leveling of field gages, lack of boundary input data from a marine model for wind-induced water slope and tides, and use of tidal harmonic characteristics derived from the Florida Bay model to create the tidal boundary conditions. The comparisons are shown in figure 18; for clarity, a 15-day period corresponding to the duration of a spring neap cycle is shown. All sites, except for the Chatham River gage, were referenced to a datum; therefore, the Chatham data cannot be used for comparisons of mean. The time-series plots show a clear decline in sea level during April 18-20, 2001, which is likely attributable to wind.

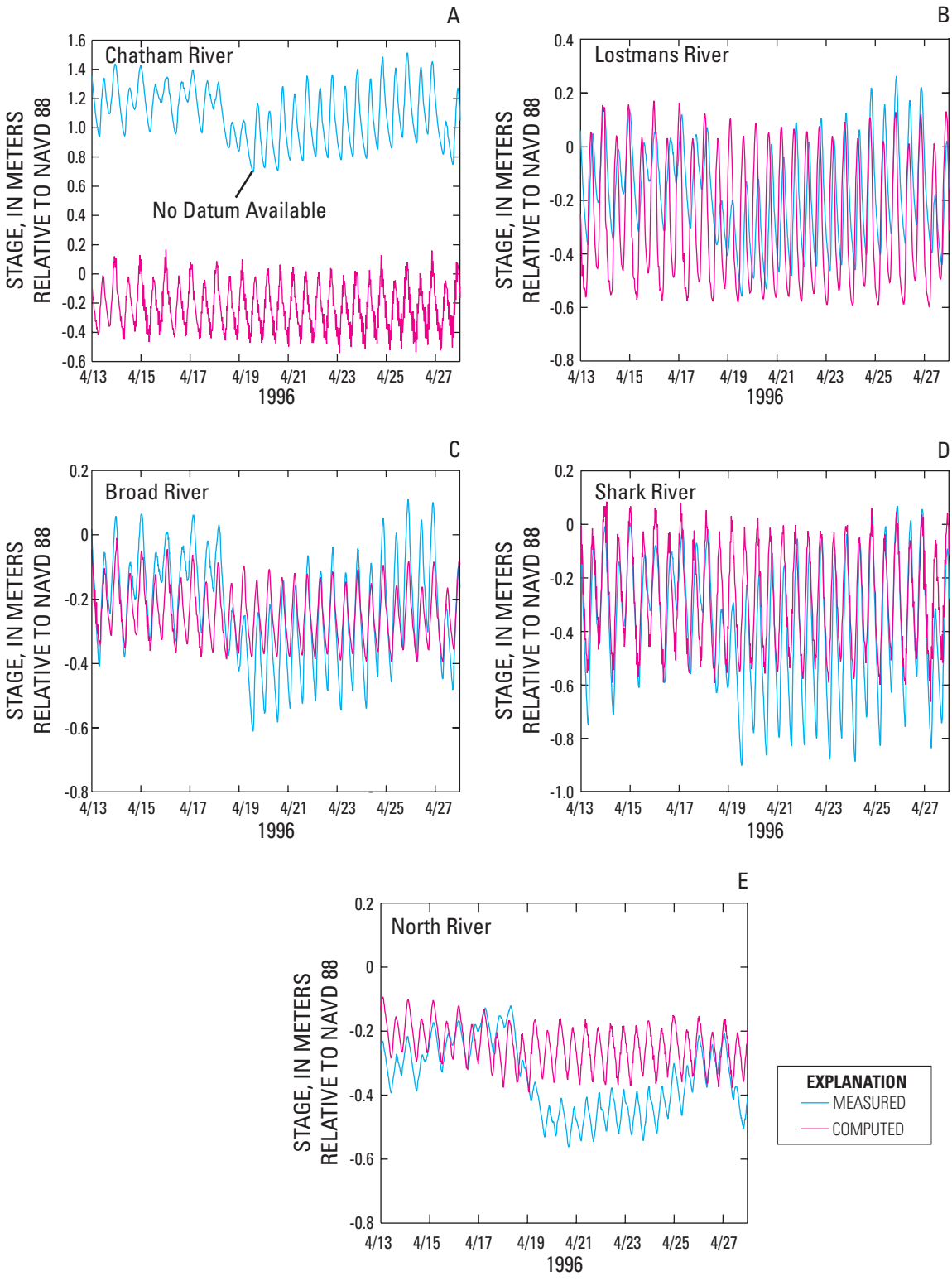

Figure 18. Measured and computed stage at selected west coast rivers over time. River locations are shown in figure 1.

Table 6. West coast river stage comparison statistics for run 142.

[Rivers are shown in figure 1]

Station	Measured stage mean (meters)	Computed stage mean (meters)	Measured stage standard deviation (meters)	Computed stage standard deviation (meters)	Percentage of explained variance	Number of points
Chatham River	1.20	-0.01	0.20	0.18	61	27,822
Lostmans River	-.02	-.06	.20	.24	40	27,554
Broad River	-.05	-.01	.18	.15	61	30,244
Shark River	-.19	-.07	.23	.19	68	29,187
North River	-.20	-.04	.12	.11	61	27,695

Wind-induced water-level slope at the boundary, however, is not prescribed in the model forcing, and the model response includes direct wind-stress effects that fail to produce a similar slope in the model. The tidal ranges and lower frequency (monthly) water-level fluctuations are captured by the model, but the spring-neap variations in diurnal tide inequalities are not as well represented. It is likely that the preliminary tidal harmonic components inadequately describe actual tides.

Base run stage comparison statistics were compiled for the five west coast river stations presented in table 6. The comparison was based on half-hourly values, and time values without valid gage data are excluded. The differences in measured means indicate further investigation is needed to resolve problems related to datum referencing at the west coast river sites. If monitoring stations are in tidal reaches of the rivers and have strong hydraulic connections with the ocean, their associated means should agree closely, and this is the case with the model means. Because preliminary boundary conditions are used, these statistics can be used to measure any improvement that results from prescribing better boundary conditions as they become available from the Florida Bay model. The PEV values at four of the five stations are greater than 0.6, however, which is satisfactory when considering the large errors that can be induced by small phase errors. The primary problem with tidal data is matching phase; a large water-level error can be caused by a small phase error. The smaller PEV at Lostmans River is most likely due to: (1) an overestimation of the standard deviation by the model, which results from representing tidal fluctuations that are too large; and (2) a model phase that leads the measured phase, particularly at low tide. These characteristics indicate that the model friction in the lower reach of Lostmans River needs to be increased to achieve a better match between measured and computed tidal water-level fluctuations.

Using the measured flows at the five west coast river stations noted earlier, an evaluation of model-predicted flows was made for the part of the Standard Data Period (SDP) for which data were available. The flow records at the different locations started at different times during 2001 and all extended beyond 2002. Owing to the constrained model resolution, it was necessary, in some instances, to approximate several rivers as one. To drain water efficiently to the coast, rivers in the model must have sufficient depths so as to not dry out at the wrong level. River cells, therefore, must have a bottom altitude representative of the river rather than the adjacent banks or an average of both. Where natural rivers lie relatively close to each other, it is difficult to implement the necessary depth along each river in the model without making the local model topography too low. For example, a number of parallel rivers are combined with the Shark and North Rivers in the model (figs. 1 and 3); all are hydraulically connected to Whitewater Bay. These approximations should yield acceptable values for runoff to the bay, even though local flow paths and flow volumes will differ somewhat from actual conditions.

Model calibration consisted of modifying model topography to assure that rivers had sufficient depth and covered enough area to allow realistic drainage as indicated by the descending phases of the stage time series. Adjustments to topography and upstream friction also were made to match model drainage to the magnitudes of net seaward flows measured at the five USGS west coast river stations. Chatham, Shark, and North Rivers were allowed to have more flow because they represented a combination of adjacent, mostly parallel rivers. Finally, the friction in the downstream sections of the rivers was adjusted to match tidal stage and flow ranges. The calibrated Manning's *n* values for the rivers are shown in figure 4.

A 15-day, neap-spring cycle period was chosen from April 23, 2001, to May 8, 2001, and flow comparisons for this period are shown in figure 19. The simulated tidal flows are in phase with the measured flows. The model overestimated the magnitude of flow at Shark and North River, and to a lesser extent, Chatham River, which is expected because all these rivers include flows of adjacent smaller rivers as previously described.

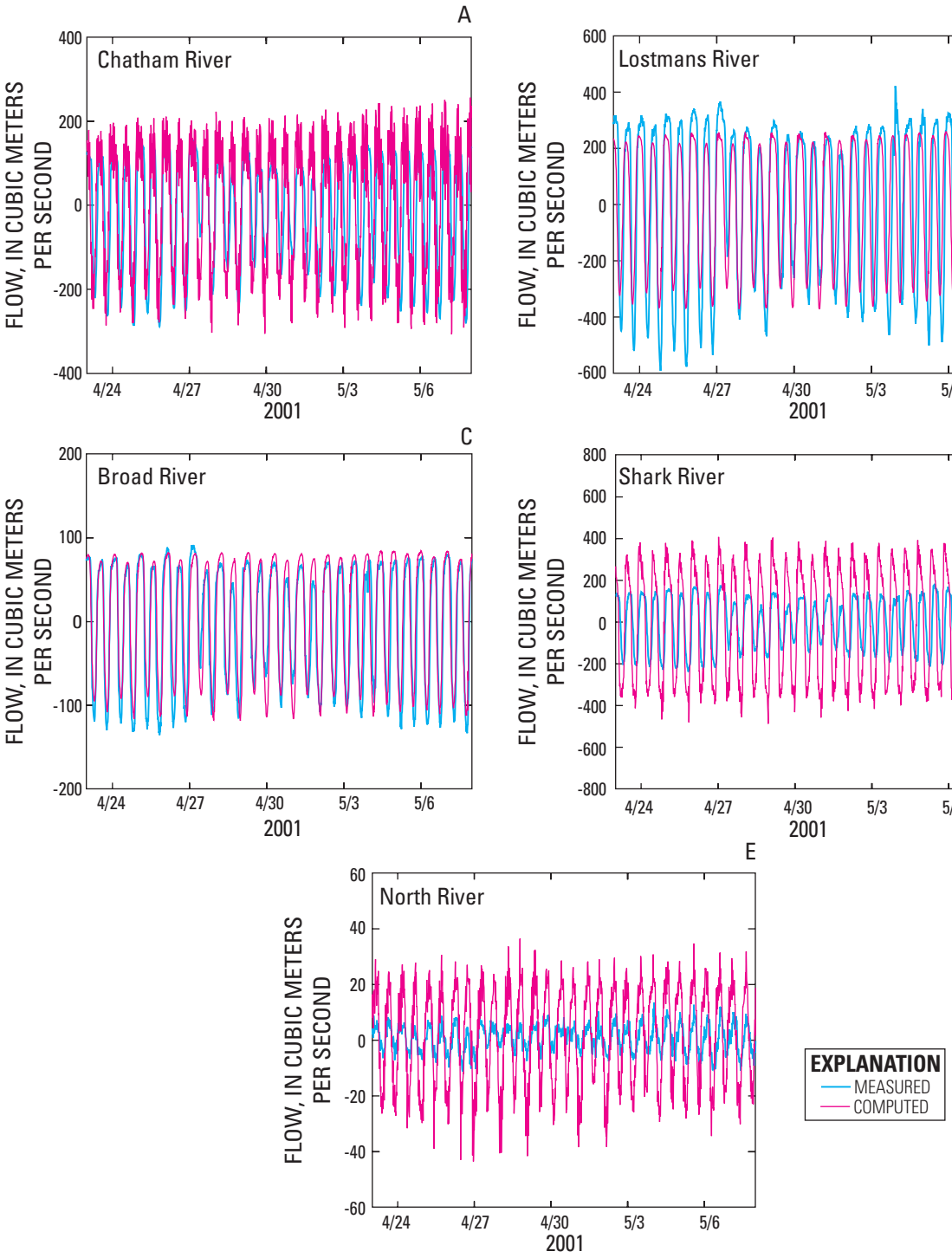

Figure 19. River flow over neap-spring cycle at selected west coast rivers. The rivers are shown in figure 1.

Flow comparison statistics were compiled for the five west coast river stations noted earlier, based on 15-minute data and ignoring missing data points (table 7). The PEV values are poor at locations corresponding to the combined rivers. The flow comparison graphs shown in figure 19 indicate, however, that PEV would improve substantially at Chatham, Shark and North Rivers if their flows were partitioned into individual rivers. The graphs of cumulative flows shown in figure 20 do not show any unusual trends; measured and computed flows show similar seasonal variations. The computed cumulative flows are consistently higher than measured cumulative flows at these three rivers because they encompass a number of smaller rivers. As noted earlier, table 2 gives the computed net average flows at gaging stations along the rivers.

Table 7. Comparison statistics for measured and computed west coast river flows.

[Rivers are shown in figure 1]

Station	Measured discharge mean (meters)	Computed discharge mean (meters)	Measured discharge standard deviation (meters)	Computed discharge standard deviation (meters)	Percentage of explained variance	Number of points
Chatham River	10.6	19.1	162.0	128.7	0.5	54,032
Lostmans River	39.2	39.1	340.4	277.6	.7	52,722
Broad River	10.3	8.3	76.7	78.6	.7	60,482
Shark River	14.1	20.3	131.2	360.7	-3.9	57,122
North River	1.9	6.8	9.2	21.5	-2.5	54,958

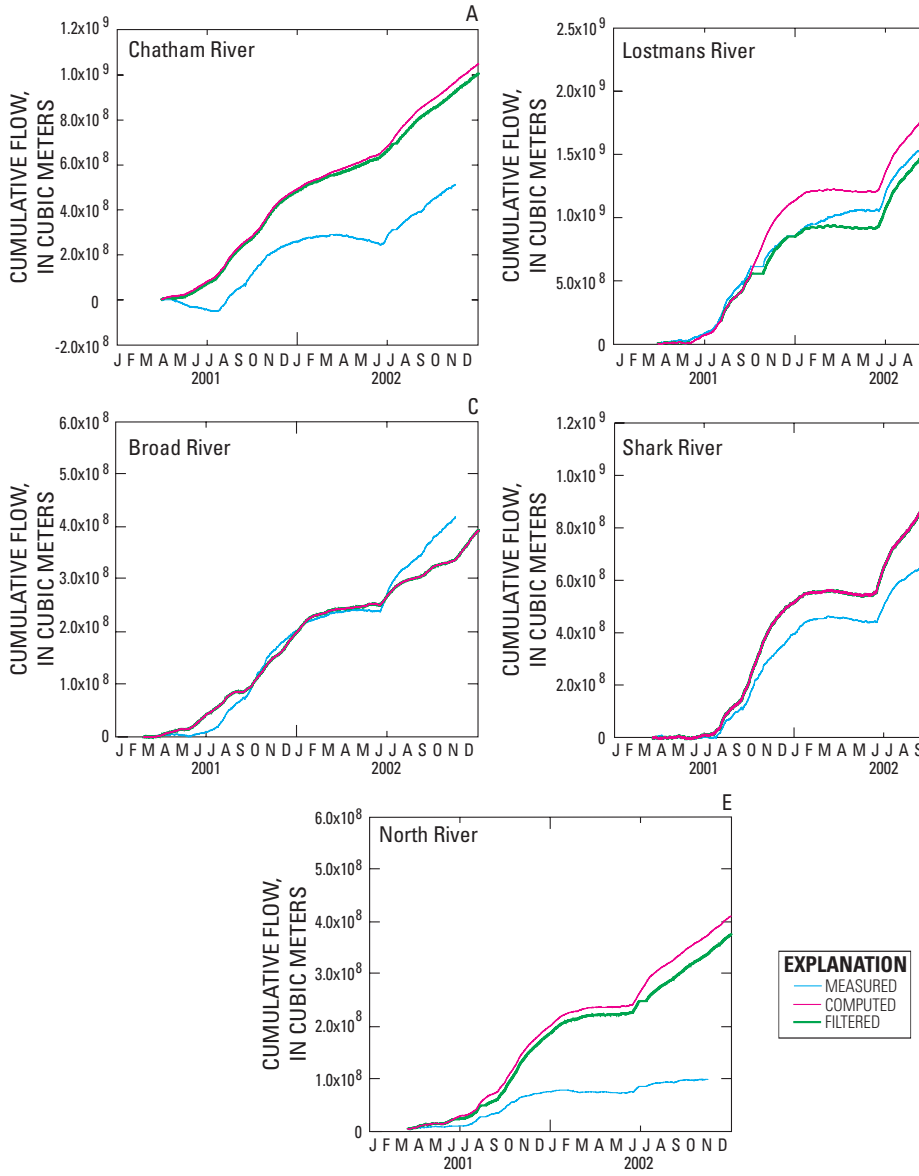

Figure 20. Cumulative flows at selected west coast rivers over time. Rivers are shown in figure 1.